

# Estimation of SynRM Flux Saturation Model at Standstill using Artificial Neural Network

Yun-Jae Lee<sup>1</sup>, Min-Seong Lee<sup>1</sup>, and Young-Doo Yoon<sup>2</sup>

<sup>1</sup> Department of Automotive Engineering Automotive-Computer Convergence, Hanyang University, Korea

<sup>2</sup> Department of Automotive Engineering, Hanyang University, Korea

**Abstract--** This paper proposes a method for estimating the magnetic flux saturation model of SynRM in a stationary state using an Artificial Neural Network (ANN). In the stationary state, the ANN is trained using the sampled current and the calculated magnetic flux obtained during hysteresis current control. The d-q axis magnetic flux generated according to the d-q axis current of SynRM appears symmetrically with respect to the axis and the origin. Using this phenomenon, the model was trained in the first quadrant by taking absolute values from the current and magnetic flux data. It was confirmed that the trained ANN model can represent the magnetic flux saturation phenomenon by comparing the estimated magnetic flux of the ANN model with the current-flux data. To verify the effectiveness of the proposed methods, the ANN flux saturation model was applied to sensorless drives with 1.5kW SynRM.

**Index Terms--** Artificial neural networks, Machine learning, Synchronous reluctance machine (SynRM), Flux maps, Identification, Saturation characteristics, Torque control, Sensorless drive.

## I. INTRODUCTION

Synchronous reluctance motors (SynRMs) generate reluctance torque based on salient rotor structures. Those have a simple structure without permanent magnets or rotor windings, which makes them reliable and cost-effective. However, due to those high saliency ratios and large inductances, SynRMs exhibit significant magnetic saturations. Thus, consideration of magnetic saturation is necessary for the high-efficiency operations of SynRMs [1]-[3].

A commonly used MTPA method is implemented by measuring the maximum torque per unit current using a dynamometer and creating lookup tables of operation points. This method takes a long time and requires a torque sensor.

Other methods are injecting a high-frequency signal [4] during operation to track the MTPA trajectory and fitting the torque per unit current equation using tests for several operating points [5] online. However, this method has the disadvantage of requiring additional signals or changing the current operating point.

MTPA lookup tables can be also written offline by performing  $\beta$ -angle calculations [6]. Recently, an optimal torque control [7] was proposed and it creates several lookup tables. This method requires the d-q axis magnetic flux saturation models  $\lambda_d(i_d, i_q)$  and  $\lambda_q(i_d, i_q)$  for the d-q axis current. Using the magnetic flux saturation models,

the d-q axis inductance can be calculated and used in sensorless controls based on the back electromotive force [8] and magnetic flux observer [9].

The magnetic flux saturation model can be estimated in the rotating state or standstill. The rotating state method is controlling the speed of a test motor while estimating the magnetic flux saturation model. A method proposed in [10] calculates the magnetic flux using voltage and current at multiple operating points and fits a current model for the magnetic flux at standstill. Magnetic flux saturation model estimation methods can be divided under locked rotor conditions [11] and methods without locking the rotor. The rotor-locked method and rotating state method require additional equipment and requirements. Therefore, to utilize the magnetic flux saturation model estimation algorithm without restriction, it is more suitable to estimate without locking the rotor. Methods for estimating the current model for the magnetic flux and the magnetic flux model for the current at standstill have been proposed for SynRM [12] and [13]. Since the magnetic flux saturation model appears nonlinear, the method of expressing the magnetic flux saturation as a mathematical model has limitations in representing the magnetic flux saturation. And it may cause errors with the actual magnetic flux saturation phenomenon.

High-accuracy models can be achieved using computational methods, such as machine learning. An artificial Neural Network (ANN) has an increased capacity to fit non-linear functions and find patterns in the acquiring data. The implementation of ANN indicates modeling the model's inputs and outputs with their connection decided by layers and training algorithms. In motor drives using ANN approaches, studies on torque ripple reduction, vector control, and saturated model prediction are being conducted [14]-[18].

ANN is suitable for predicting a nonlinear model that is difficult to represent. It can be applied to predicting a magnetic flux saturation model that appears nonlinear due to the inductance saturation of the motor. However, because the required amount of operation in the learning and calculation process is very large, operations using FPGA or PCs might be required for motor drives [19].

In this paper, ANN was used to implement the nonlinear magnetic flux saturation of SynRM as a multi-layer model. The structure of the ANN was selected considering the form of the magnetic flux saturation and the computation time of DSP. For the training data, the preprocessing method was used to improve the training accuracy of ANN considering the tendency of the magnetic flux saturation of

SynRM. To verify the trained ANN flux model, sensorless control based on a magnetic flux observer [9] was performed with 1.5kW SynRM.

## II. SYNRM MODEL AND DATA ACQUISITION

### A. Fundamental Equations

The SynRM model is considered in the rotor reference frame. The stator voltage equations are

$$\frac{d\lambda_{ds}^r}{dt} = v_{ds}^r - R_s i_{ds}^r + \omega_r \lambda_{qs}^r, \quad (1a)$$

$$\frac{d\lambda_{qs}^r}{dt} = v_{qs}^r - R_s i_{qs}^r - \omega_r \lambda_{ds}^r \quad (1b)$$

where  $\lambda_{ds}^r$  and  $\lambda_{qs}^r$  are d-q axis magnetic flux linkages.  $v_{ds}^r$  and  $v_{qs}^r$  are d-q axis voltages.  $i_{ds}^r$  and  $i_{qs}^r$  are d-q axis currents.  $\omega_r$  is the electrical angular speed of the rotor. Torque is given by

$$T_e = \frac{3P}{2} (\lambda_{ds}^r i_{qs}^r - \lambda_{qs}^r i_{ds}^r). \quad (2)$$

### B. Data Acquisition

To collect d-q axis current and magnetic flux data for ANN training, hysteresis current control is performed. Hysteresis current control is divided into three stages and the output voltage is controlled as shown in (3). First, in order to find out the d-axis magnetic saturation, a voltage reference is applied only to the d-axis and the q-axis voltage is zero. Second, a voltage reference is applied only on the q-axis to measure the q-axis magnetic saturation. Finally, voltage references are simultaneously applied to the d and q axis to measure the cross-saturation (3) effects. For accurate measurements, mitigation techniques for rotor movement [13] can be used.

$$u_{inj}(k) = \begin{cases} u_{mag}, & \text{if } i(k) < -i_{max} \\ -u_{mag}, & \text{if } i(k) > i_{max}, \\ u_{inj}(k-1), & \text{otherwise} \end{cases} \quad (3)$$

$$u_{ref}(k) = u_{inj}(k) + R_s i(k)$$

The magnetic fluxes are calculated from the current and voltage data acquired. Since the hysteresis current control is performed in a stationary state,  $\omega_r$  can be assumed as zero, and the d-q axis magnetic flux is expressed as

$$\lambda_{ds} = \int u_{ds} - R_s i_{ds} dt, \quad (4a)$$

$$\lambda_{qs} = \int u_{qs} - R_s i_{qs} dt. \quad (4a)$$

## III. TRAINING ARTIFICIAL NEURAL NETWORK

### A. Artificial Neural Network Model

The multi-layer ANN and backpropagation method have often been used in model identification studies. ANN usually consists of nodes, and activation functions, that conn a number of layers and elements. In (5), X, W, and b

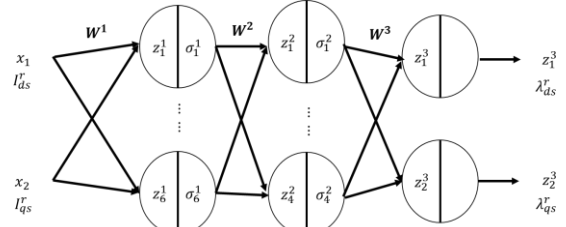


Fig. 1. ANN flux saturation model

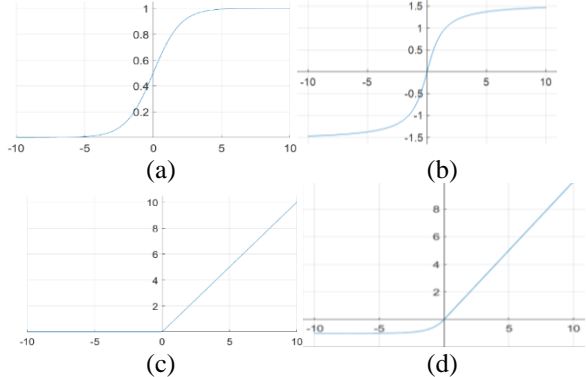


Fig. 2. Activation function; (a) sigmoid (b) hyperbolic tangent (c) ReLU (d) ELU

mean input, weight, and bias, respectively  $\sigma$  is the activation function. Equation (5a) represents the sum of the multiplied weights with input and bias, and (5b) represents the output of the layer that (5a) apply to the activation function.

In Fig. 1, the superscripts of Z and  $\sigma$  indicate the hidden layer order, and the subscript indicates the order of the node within the layer.

Each layer has an activation function at the output. But in the output layers, activation functions were not used because the ANN flux saturation model is not a classification model but a model for regression analysis. Since magnetic fluxes and currents are continuous data and the purpose is to find a correlation between the two, an activation function is not used in the output layer when constructing a model.

$$Z = \sum Wx + b, \quad (5a)$$

$$Y = \sigma(Z). \quad (5b)$$

In this study, the input of the ANN model is current, and the output is magnetic flux. The model consists of 1 input layer, 2 hidden layers, and 1 output layer. If the hidden layer is composed of only one layer, the magnetic flux saturation model is not well represented nonlinearly due to the high magnetic flux saturation phenomenon of SynRM. Also, if the model is too simple, there is a risk of underfitting the training data [21].

### B. Decision of Activation Function

The activation functions represent the nonlinearity of the model. Layers are expressed as linear expressions and use an activation function to generate nonlinearity. Therefore, the shape of the learned model is greatly

influenced by the shape of the activation function. To express the magnetic flux saturation phenomenon, the selection of an activation function is very important. Fig. 2 shows the four functions that were reviewed to select the activation function to be used in the ANN. It was selected considering the advantages and disadvantages of each function.

The hyperbolic tangent function as (6) has a shape that is similar to the magnetic flux saturation model and passes the origin. However, as shown in (6), this function shows a slower learning rate than sigmoid because it requires more calculations of the exponential function.

$$\tanh(x) = \frac{e^x - e^{-x}}{e^x + e^{-x}}. \quad (6)$$

In the case of the ReLU function of (7), it shows faster training speed and lower computational burden. From the perspective of DSP, which is limited in computational speed and time, this is a strong advantage. However, when the model is trained using ReLU with limited data, a rough and curved surface appears as shown in Fig. 3. Because of the shape of the function as shown in Fig. 2 (c). Rough surfaces increase the calculation error of inductance. This rough surface can be finely represented as the layers increase. When the input of the activation function increases, the output of the activation function is outputted as much as the input. The magnetic flux saturation model cannot avoid the large difference in input and output values, resulting in gradient explosion. To prevent this, additional algorithms are needed. An increased number of layers cause increased computational time. Thus, the ReLU function is unsuitable.

$$ReLU(x) = \begin{cases} x, & x > 0 \\ 0, & \text{otherwise}. \end{cases} \quad (7)$$

The ELU function of (8) is expressed as an exponential function for negative inputs and is continuous around zero so that it is differentiable. The function shape is also smooth as shown in Fig. 2 (d), so the trained model plane appears smooth, and a small number of layers are required. In addition, the computational cost is smaller than the sigmoid function. However, there is a risk of gradient explosion in the positive part like the ReLU function. Therefore, additional algorithms are needed to prevent this, and overall computation time may increase.

$$ELU(x) = \begin{cases} x, & x > 0 \\ \alpha \cdot (e^x - 1), & \text{otherwise}. \end{cases} \quad (8)$$

In the case of the sigmoid function (9), this function has a very similar shape of the magnetic flux saturation model and can represent the magnetic flux saturation phenomenon well because the function shape changes smoothly. However, the sigmoid function has a problem of vanishing gradient [22]. But this problem can be avoided

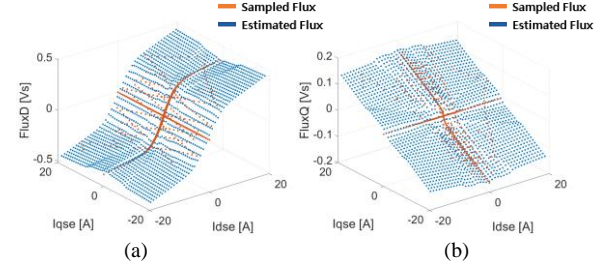


Fig. 3. 10x10x10 ANN flux saturation model, using ReLU; (a) d-axis; (b) q-axis.

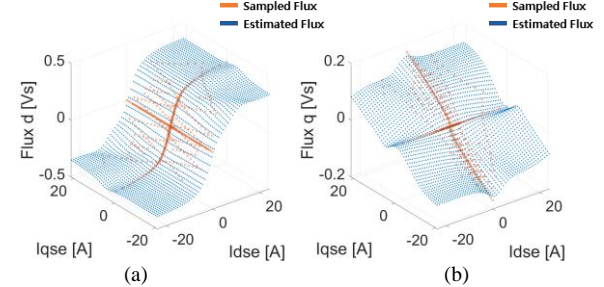


Fig. 4. 6x4 ANN flux saturation model trained by Symmetric transform with Sigmoid; (a) d-axis (b) q-axis.

because the number of layers used in this study is small. Furthermore, sigmoid does not require additional algorithms such as normalization or gradient clipping to prevent gradient exploding, since the output converges to nearly 1 even as the input value increases. since the sigmoid function outputs a continuous value for the output as shown in Fig. 2 (a), it is differentiable around zero and the learned model is well expressed continuously.

$$\text{sigmoid}(x) = \frac{1}{1+e^{-x}}. \quad (9)$$

### C. Data Preprocessing

Artificial neural network (ANN) learns from given data and may reflect the tendency in the surrounding areas or produce very different results for areas without data. If the model is too simple compared to the data, underfitting occurs, while selecting complex model results in overfitting. Therefore, the number and location of data points are crucial in learning.

Since SynRM does not have a permanent magnet, the saturation model becomes symmetric about the origin in the current and magnetic flux relationship. To mitigate the lack and imbalance of training data, this paper symmetrically collected and trained the model with training data in one quadrant and flipped the sign of the model output when predicting.

The model trained using this method, as shown in Fig. 4, is symmetric about the origin, but exhibits a strong curvature around the vicinity where the d-axis or q-axis currents are zero. This is because, when the data is symmetric about the origin, there exists a data imbalance in the vicinity of zero for only one quadrant. To solve this problem, data was mirrored about the origin, and additional current data about 0.3 p.u. was added to the opposite plane around the zero point. By adding additional

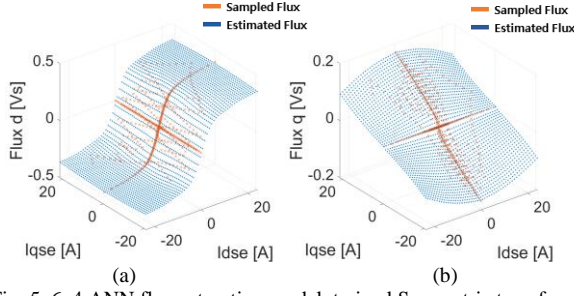


Fig. 5. 6x4 ANN flux saturation model, trained Symmetric transform adding data around axis with Sigmoid; (a) d-axis (b) q-axis.

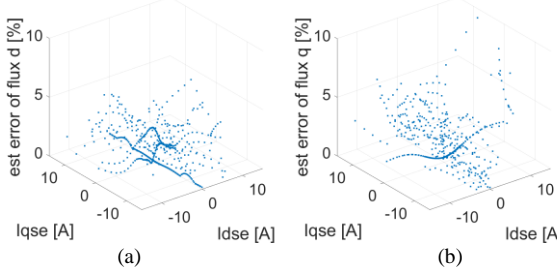


Fig. 6. error rate of ANN flux saturation model; (a) d-axis (b) q-axis.

data near the zero points, the training of the model was less influenced by self-saturation. As for the number of data, if the data is concentrated in one part, the tendency of the concentrated part is very strong, so it is better to arrange the similar number of data as possible.

As a result of adding data near the d-q axis, the distortion disappeared around the d-q axis, as shown in Fig. 5. Fig. 6 shows the calculated error rate between the raw data and the ANN flux saturation model. The error rate of the d-axis magnetic flux is within 5%. The error rate of the q-axis magnetic flux shows less than 5% in high current and less than 10% in other areas. The model seems to express the magnetic flux saturation phenomenon well, even in the high current section.

#### IV. EXPERIMENTAL RESULTS

##### A. Data Acquisition

Experiments with 1.5kW SynRM were performed with the M-G set shown in Fig. 7. In Fig. 8, d-axis current and magnetic flux data were collected. q-axis current and magnetic flux data collected. Lastly, data for cross saturation were acquired. It can be seen that the motor angle hardly changed during the data collection process, indicating that the data was collected with minimal distortion. By hysteresis current control test, 550 data were collected. After preprocessing, 660 data were used for training.

##### B. ANN Flux Saturation Model

The ANN flux saturation Model was trained using python and verified using Matlab to check the accuracy of the model's plane and error. After that, the ANN flux saturation model was applied to DSP for the calculation of inductance.

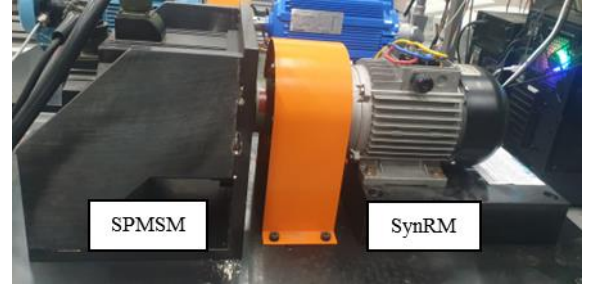


Fig. 7. Experimental setup of 1.5kW under test

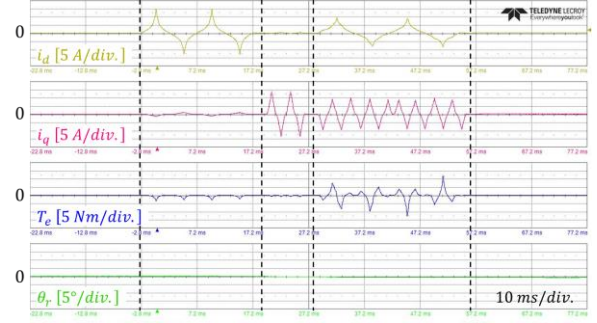


Fig. 8. Hysteresis current control waveform

TABLE I  
NOMINAL PARAMETERS OF THE TESTED SYNRM

Parameter	Value [Unit]
Rated power	1.5 [kW]
Pole pair	2
Rated speed	3000 [r/min]
Rated torque	4.48 [Nm]
Rated voltage	210 [ $V_{rms}$ ]
Rated current	7.5 [ $A_{rms}$ ]
Stator resistance	1.2802 [ $\Omega$ ]
d-axis inductance	78 [mH]
q-axis inductance	20 [mH]

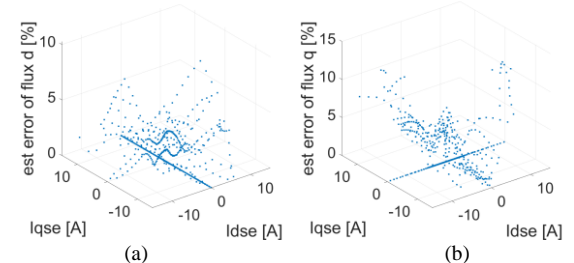


Fig. 9. Error rate of formula-based model; (a) d-axis, (b) q-axis.

TABLE II  
FITTED PARAMETERS OF SYNRM

$A_d$	$B_d$	$C_d$
0.2403	0.3399	0.0028
$A_q$	$B_q$	$C_q$
0.0422	0.1841	0.0052
$K_d$	$K_q$	$D_{dq}$
225	225	-0.9198

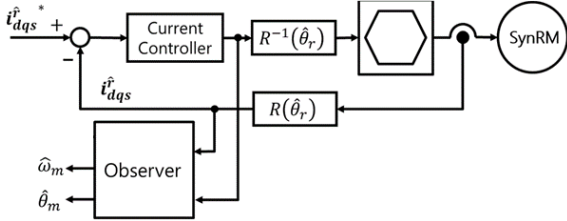


Fig. 10. Sensorless control system

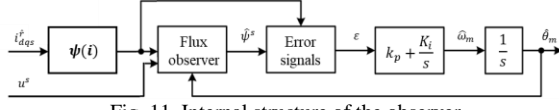


Fig. 11. Internal structure of the observer

### C. Formula-based equation for comparison

The magnetic flux saturation model proposed in [20] was used as a comparison group against the ANN flux saturation Model. This model is fitted through the current and magnetic flux data. The equation is the same as (10), and the coefficients are shown in Table II. These equations are models in which the input is current, and the output is magnetic flux, the same as the ANN flux saturation model. The A, B, and C coefficients in (10) represent the terms for self-axis saturation, while the D and K coefficients represent the terms for cross-saturation. As shown in Fig. 9, the magnetization is well represented in the low current range, but the error increases to more than 10% as the current increases.

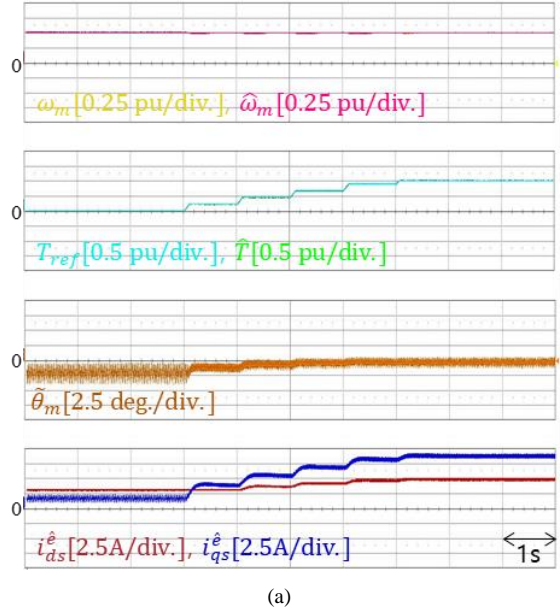
$$\lambda_d(i_d, i_q) = A_d \tan^{-1}(B_d i_d) + C_d i_d + \frac{D_{dq} i_d}{i_d^2 + K_d} \ln(1 + \frac{i_q^2}{K_q}). \quad (10a)$$

$$\lambda_q(i_d, i_q) = A_q \tan^{-1}(B_q i_q) + C_q i_q + \frac{D_{dq} i_q}{i_q^2 + K_q} \ln(1 + \frac{i_d^2}{K_d}). \quad (10b)$$

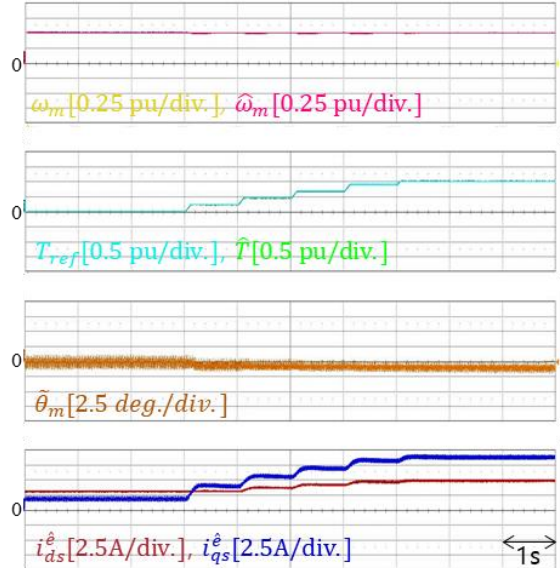
### D. Sensorless Control Using ANN Flux Model

To verify the performance of the measured ANN flux saturation model, sensorless control using a magnetic flux observer [9] was performed. And the internal magnetic flux saturation model in the magnetic flux observer was replaced with the ANN flux saturation model as shown in Fig. 11. The performance of the model was compared with that of the formula-based model [20].

The experiments were performed at the speed of 0.5 p.u., with loads ranging from no load to the rated load. It was implemented in TMS320F28377S. During the experiment, a switching frequency of 5 kHz and a sampling frequency of 10 kHz were used. As shown in Fig. 12, the sensorless control using the ANN flux saturation model showed an angular error of 1.2° at a low current region, but in the high current region, the angular error decreased to 0.1°, while using the formula-based model showed an angular error of 1.2°. It can be confirmed that the ANN flux saturation model represents the magnetic flux more accurately in the high current region. However, the ANN flux saturation model shows more errors in the low current region near zero.



(a)



(b)

Fig. 12. Experimental results showing angle error; (a) ANN flux saturation model (b) formula-based model flux saturation model.

## V. CONCLUSIONS

This paper proposes an ANN flux saturation model for the magnet flux saturation model of SynRMs. Considering the magnetic flux model of SynRM, the preprocessing for data was conducted. And activation function was selected by considering the tendency and shape of the ANN flux saturation model plane. Apparent inductance and dynamic inductance can be computed by the ANN flux saturation model. The calculated inductances were used in the magnetic flux observer for sensorless drives. To verify the ANN flux saturation model, a comparison with raw data and sensorless control was conducted. The experimental results of sensorless drives were acceptable, presenting the angle error of sensorless drive was about 0.1°~1.2°.

## ACKNOWLEDGMENT

This paper was supported by the Korea Institute for Advancement of Technology(KIAT) grant funded by the Korea Government(MOTIE)(P0020536, The Competency Development Program for Industry Specialist)

## REFERENCES

- [1] A. Yousefi-Talouki, P. Pescetto and G. Pellegrino, "Sensorless Direct Flux Vector Control of Synchronous Reluctance Motors Including Standstill, MTPA, and Flux Weakening," in IEEE Transactions on Industry Applications, vol. 53, no. 4, pp. 3598-3608, July-Aug. 2017, doi: 10.1109/TIA.2017.2679689.
- [2] A. Accetta, M. Cirrincione, M. C. D. Piazza, G. L. Tona, M. Luna and M. Pucci, "Analytical Formulation of a Maximum Torque per Ampere (MTPA) Technique for SynRM<sub>s</sub> Considering the Magnetic Saturation," in IEEE Transactions on Industry Applications, vol. 56, no. 4, pp. 3846-3854, July-Aug. 2020, doi: 10.1109/TIA.2020.2993525.
- [3] W. Lee, J. Kim, P. Jang and K. Nam, "On-Line MTPA Control Method for Synchronous Reluctance Motor," in IEEE Transactions on Industry Applications, vol. 58, no. 1, pp. 356-364, Jan.-Feb. 2022, doi: 10.1109/TIA.2021.3128468.
- [4] S. Kim, Y. Yoon, S. Sul and K. Ide, "Maximum Torque per Ampere (MTPA) Control of an IPM Machine Based on Signal Injection Considering Inductance Saturation," in IEEE Transactions on Power Electronics, vol. 28, no. 1, pp. 488-497, Jan. 2013, doi: 10.1109/TPEL.2012.2195203.
- [5] G. Feng, C. Lai, Y. Han and N. C. Kar, "Fast Maximum Torque Per Ampere (MTPA) Angle Detection for Interior PMSMs Using Online Polynomial Curve Fitting," in IEEE Transactions on Power Electronics, vol. 37, no. 2, pp. 2045-2056, Feb. 2022, doi: 10.1109/TPEL.2021.3109112.
- [6] S. Morimoto, K. Hatanaka, Y. Tong, Y. Takeda and T. Hirasa, "Servo drive system and control characteristics of salient pole permanent magnet synchronous motor," in IEEE Transactions on Industry Applications, vol. 29, no. 2, pp. 338-343, March-April 1993, doi: 10.1109/28.216541.
- [7] H. A. A. Awan, Z. Song, S. E. Saarakkala and M. Hinkkanen, "Optimal Torque Control of Saturated Synchronous Motors: Plug-and-Play Method," in IEEE Transactions on Industry Applications, vol. 54, no. 6, pp. 6110-6120, Nov.-Dec. 2018, doi: 10.1109/TIA.2018.2862410.
- [8] S. Morimoto, K. Kawamoto, M. Sanada, and Y. Takeda, "Sensorless control strategy for salient-pole PMSM based on extended EMF in rotating reference frame," IEEE Transactions on Industry Applications, vol. 38, doi: 10.1109/TIA.2002.800777, no. 4, pp. 1054-1061, Jul.-Aug. 2002.
- [9] T. Tuovinen, H. A. Ali Awan, J. Kukkola, S. E. Saarakkala, and M. Hinkkanen, "2018 IEEE 9th International Symposium on Sensorless Control for Electrical Drives (SLED)," in Permanent-Magnet Flux Adaptation for Sensorless Synchronous Motor Drives, doi: 10.1109/SLED.2018.8485899, pp. 138-143, 2018.
- [10] Z. Qu, T. Tuovinen and M. Hinkkanen, "Inclusion of magnetic saturation in dynamic models of synchronous reluctance motors," 2012 XXth International Conference on Electrical Machines, 2012, pp. 994-1000, doi: 10.1109/ICEIMach.2012.6349997.
- [11] A. Varatharajan, P. Pescetto and G. Pellegrino, "Sensorless Self-Commissioning of Synchronous Reluctance Machine with Rotor Self-Locking Mechanism," 2019 IEEE Energy Conversion Congress and Exposition (ECCE), 2019, pp. 812-817, doi: 10.1109/ECCE.2019.8913023.
- [12] M. Hinkkanen, P. Pescetto, E. Mölsä, S. E. Saarakkala, G. Pellegrino and R. Bojoi, "Sensorless self-commissioning of synchronous reluctance motors at standstill," 2016 XXII International Conference on Electrical Machines (ICEM), 2016, pp. 1174-1180, doi: 10.1109/ICELMACH.2016.7732673.
- [13] H. -J. Lee, J. -E. Joo and Y. -D. Yoon, "Standstill Sensorless Self-Commissioning Strategy of Synchronous Machine Considering Rotor Rotation Reduction Technique," 2022 International Power Electronics Conference (IPEC-Himeji 2022- ECCE Asia), Himeji, Japan, 2022, pp. 2694-2700, doi: 10.23919/IPEC-Himeji2022-ECCE53331.2022.9807050.
- [14] S. Pillutla and A. Keyhani, "Neural network based saturation model for round rotor synchronous generator," in IEEE Transactions on Energy Conversion, vol. 14, no. 4, pp. 1019-1025, Dec. 1999, doi: 10.1109/60.815022.
- [15] S. Li, H. Won, X. Fu, M. Fairbank, D. C. Wunsch and E. Alonso, "Neural-Network Vector Controller for Permanent-Magnet Synchronous Motor Drives: Simulated and Hardware-Validated Results," in IEEE Transactions on Cybernetics, vol. 50, no. 7, pp. 3218-3230, July 2020, doi: 10.1109/TCYB.2019.2897653.
- [16] D. Flieller, N. K. Nguyen, P. Wira, G. Sturtzer, D. O. Abdeslam and J. Mercklé, "A Self-Learning Solution for Torque Ripple Reduction for Nonsinusoidal Permanent-Magnet Motor Drives Based on Artificial Neural Networks," in IEEE Transactions on Industrial Electronics, vol. 61, no. 2, pp. 655-666, Feb. 2014, doi: 10.1109/TIE.2013.2257136.
- [17] Chich-Yi Huang, Tien-Chi Chen and Ching-Lien Huang, "Robust control of induction motor with a neural-network load torque estimator and a neural-network identification," in IEEE Transactions on Industrial Electronics, vol. 46, no. 5, pp. 990-998, Oct. 1999, doi: 10.1109/41.793348.
- [18] C. Li, J. Xiong, X. Zhu, Q. Zhang and S. Wang, "Fault Diagnosis Method Based on Encoding Time Series and Convolutional Neural Network," in IEEE Access, vol. 8, pp. 165232-165246, 2020, doi: 10.1109/ACCESS.2020.3021007.
- [19] M. R. Raia, M. Ruba, R. O. Nemes and C. Martis, "Artificial Neural Network and Data Dimensionality Reduction Based on Machine Learning Methods for PMSM Model Order Reduction," in IEEE Access, vol. 9, pp. 102345-102354, 2021, doi: 10.1109/ACCESS.2021.3095668.
- [20] T. -G. Woo, S. -W. Park, S. -C. Choi, H. -J. Lee and Y. -D. Yoon, "Flux Saturation Model Including Cross Saturation for Synchronous Reluctance Machines and Its Identification Method at Standstill," in IEEE Transactions on Industrial Electronics, vol. 70, no. 3, pp. 2318-2328, March 2023, doi: 10.1109/TIE.2022.3174233.
- [21] L. Ali, A. Rahman, A. Khan, M. Zhou, A. Javeed and J. A. Khan, "An Automated Diagnostic System for Heart Disease Prediction Based on  $\chi^2$  Statistical Model and Optimally Configured Deep Neural Network," in IEEE Access, vol. 7, pp. 34938-34945, 2019, doi: 10.1109/ACCESS.2019.2904800.
- [22] Y. Bengio, P. Simard and P. Frasconi, "Learning long-term dependencies with gradient descent is difficult," in IEEE Transactions on Neural Networks, vol. 5, no. 2, pp. 157-166, March 1994, doi: 10.1109/72.279181.